Polymer-Based Optical Waveguide Tactile Sensing Method for 3-D Surfaces

Jian Hu, Danqian Cao, Yue Li, and Hongbin Liu

***Abstract*—At present, most tactile sensors are fabricated based on the flat surface, which greatly limits their applications in the 3-D scenario. To deal with the bottleneck, this article proposes a polymer-based optical waveguide sensing method. The waveguide can be integrally formed along a channel within a 3-D surface. Microbending light loss of a waveguide is the sensing principle. By studying the linearity between the degree of microbending and light loss, the feasibility analysis of spherical tactile sensing element (tactile) was completed, as well as the basis for size selection of it. In addition, the key to layout on 3-D surface of the proposed sensing method is that the bending radius of the waveguide is within the critical angle of total internal reflection (TIR). By normalizing the ratio of the side length of the cross section to the bending radius, it is shown that the light loss does not increase when the proportionality coefficient is less than 0.3. The experiment is validated by embedding four tactiles in a 3-D surface. The cross section of the waveguide is 1.5 × 1.5 mm. We demonstrated that the static hysteresis error for a tactile is less than 16% within 595 kPa, the best sensing sensitivity is 1.42 × 10^{-5} kPa^{-1}, and the maximum measurement range is from 0 to 850 kPa. As for the dynamic measurement, the tactile can rapidly response the signal change with given frequencies (the maximum is 10 Hz). The average delay time is around 12 ms.**

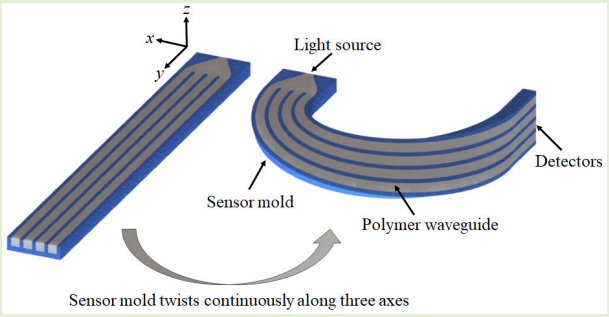

***Index Terms*—3-D surface, polymer-based, soft waveguide, tactile sensor.**

I. Introduction

TACTILE sensing is one of the key technologies in robotics to better perceive and manipulate the surrounding environment, especially for noncooperate targets [1]. To solve the challenge, various tactile sensing methods have been developed over the last decades, taking inspiration from the human sense of touch [2].

Manuscript received 19 December 2022; revised 7 February 2023; accepted 28 February 2023. Date of publication 13 March 2023; date of current version 14 April 2023. This work was supported in part by Huaiwei Technologies Research and Development (U.K.) Ltd., and in part by InnoHK Funding Scheme. The associate editor coordinating the review of this article and approving it for publication was Dr. Yong Zhu. *(Corresponding author: Hongbin Liu.)*

Jian Hu is with the Institute of Automation, Chinese Academy of Sciences (CASIA), Beijing 100190, China, and also with the Centre for Artificial Intelligence and Robotics (CAIR), Hong Kong Institute of Science and Innovation, Chinese Academy of Sciences, HongKong, China (e-mail: hujian@ia.ac.cn).

Danqian Cao and Yue Li are with School of Biomedical Engineering and Imaging Sciences, Faculty of Life Sciences and Medicine, King's College London, SE1 7EU London, U.K. (e-mail: danqian.cao@kcl.ac.uk; yue.3.li@kcl.ac.uk).

Hongbin Liu is with the Institute of Automation, Chinese Academy of Sciences (CASIA), Beijing 100190, China, also with the Centre for Artificial Intelligence and Robotics (CAIR), Hong Kong Institute of Science and Innovation, Chinese Academy of Sciences, HongKong, China, and also with the School of Biomedical Engineering and Imaging Sciences, Faculty of Life Sciences and Medicine, King's College London, SE1 7EU London, U.K. (e-mail: liuhongbin@ia.ac.cn).

Digital Object Identifier 10.1109/JSEN.2023.3252263

According to the number of sensing elements, tactile sensors can be divided into two categories, including single-point contact sensor and high spatial resolution tactile array [3]. The latter has attracted more attention due to its significant advantages, such as identifying the shape of objects via less manipulation, improving grasping stability, judging the sliding speed, and providing higher spatial resolution. Currently, the array tactile sensing technologies are mostly limited to the correspondence between pressure and electrical signals, such as voltage [4], resistance [5], or capacitance [6]. The insufficient capabilities of anti-electromagnetic and anti-humidity, together with the problems of signal drifting and complex wiring, make these types of sensors difficult to integrate with high density.

As for optical-based tactile sensing technologies, tactile information is usually measured by changes in wavelength or light intensity. Based on the former principle, a single-mode optical fiber is generally used to realize quasi-distributed sensing (such as fiber Bragg grating and Fabry–Perot cavity) or distributed sensing (such as optical frequency-domain reflectometry and Brillouin optical frequency-domain reflectometry) [7]. The above optical fiber must be fixed to the substrate, and a torsion along fiber axis is easy to produce, affecting sensor accuracy. The difficulty of measuring torsion makes this sensing method unsuitable for complex surfaces. Moreover, required optical components, such as coherent light

source and wavelength demodulation, are sophisticated and costly. By contrast, tactile sensors that rely on changes in light intensity generally only need to use a camera [8], [9], [10] or multimode optical fiber [11], [12] as a signal detector. The camera can be used to detect the deformation of elastic sensing element. Within the resolution of a camera, all deformation information in the field of view can be effectively observed, which is proper for distributed pressure measurement. However, the thickness of the sensor is large due to the built-in camera, limiting its application scenarios. The sensor that based on multimode optical fibers can transmit the change in light intensity caused by the deformation of the elastomer to the information processing module through fibers, thus avoiding the above challenge. However, if the number of tactiles is large, it will face complex wiring problem.

Although tactile sensors have been greatly improved in terms of miniaturization, integration, sensitivity, resolution, and so on, it is still a huge challenge to integrate them into devices with complex 3-D surfaces. At present, tactile sensing elements can only be mounted in a flat or cylinder surface [13], [14]. Consequently, the working space is confined, and its adaptability is insufficient in practical applications.

Some researchers solved the layout of tactile sensing elements on the 3-D surface by cutting and splicing, that is, by splicing multiple single [15] or array [16] sensors into the e-skin. Because of the need to consider wiring and communication issues, it is also not suitable for the carrier with large area.

In order to effectively integrate tactile perception on complex 3-D surfaces, another solution is to increase the flexibility of the sensors so that the electronic components can perfectly fit on the surface of the carrier under any deformation, such as bending, stretching, and shearing, and maintain the mechanical and electrical performance. In general, there are two ways to achieve flexibility [17].

1) Using soft materials such as conductive polymers and fabrics, elastomer composites with conductive filler particles, and fluids [18].

2) Using stretchable structure such as serpentine structures for interconnects or wires [19], kirigami engineered patterns to impart the electrodes a tunable elasticity [20] and so on, whereas, due to the complexity of the circuit layout, applications are limited to the smooth and regular surfaces with small curvature [21].

Another challenge for complex surface tactile sensing is long-term measurement accuracy since stress concentration may exist on the contact points or area between tactile sensors and the attached surfaces. One of the solutions is to fabricate the profile conformal tactile sensor on irregular surface [22]. Based on the sensing technology of triboelectric–photonic, a conformal e-skin was integrated on a robot hand even including the joints so that the bending of three joints on each finger and the multipoint contact on the rest area of the finger are responded on the photocurrent and voltage, respectively [23]. Similarly, Yu et al. [24] proposed a hybrid piezoelectric–triboelectric sensor that can be taped to the wrist to sense the weak pulse wave in real time. Furthermore, 3-D printing with the novelty characteristics of multimaterial and multiscale provides a flexible method to fabricate the complex structures directly and conformally onto the freeform surfaces [25]. Apart from the conformability, thinner bending thickness and stronger adhesion to soft tissues also play significant roles in measuring the biological signals accurately [26]. The "ionic gel skin" in [27] showed the super adhesiveness on various surfaces, such as skin, fluting paper, and glass, which was produced by the combination of H-bond, dynamic covalent bonds, and chemical cross-linkers. However, hysteresis and nonlinearity are the main drawbacks. The manufacturing processes of such sensors are also extraordinarily complex. Generally, technologies, such as photo-patterning and solution deposition [28], are involved. The corresponding equipment is expensive. A comparison of several typical sensors that can be applied for 3-D surface is listed in Table I.

TABLE I
COMPARISON OF SENSORS THAT CAN BE MOUNTED ON 3-D SURFACES

Applicable surfaces	Conformability	Sensitivity	Dynamic	Typical sensors
Complex 3D surface	Very high	1.42 $\times 10^{-5} kPa^{-1}$	10Hz	Proposed sensor
Flat surface or simple 3D surface	Low	412nV/N	1.49Hz	[13]
Robot hand	Low	--	--	[14, 16]
Wrist	High	--	10Hz	[19]
Back of a finger	Medium	34 mV/Pa	2Hz	[22]
Above the radial artery	Medium	15.43 /kPa	5Hz	[23]
Above the radial artery	Medium	--	1Hz	[24]

To solve the challenge associated with 3-D complex surfaces, our group has been committed to the development of a novel polymer-based optical waveguide tactile sensing technique, by embedding soft and optical transparent material channels into a given structure. Based on it, the proposed sensor is fabricated on a 3-D surface that cannot be perfectly mapped from a flat surface by bending and twisting. Tactile information can be obtained by measuring the light loss of each channel via pressuring the tactile to cause the microbending of a waveguide. Sensor performances, such as sensing sensitivity, repeatability, hysteresis curve, dynamic response, crosstalk, and maximum measurement range, are also discussed.

II. SENSOR CONCEPTS

A. Working Principle and Sensor Design

1) Total Internal Reflection (TIR): The polymer-based optical waveguide has the same principle with an optical fiber, consisting of core and cladding. The core that has a higher reflective index is surrounded by cladding. Total internal reflection (TIR) will occur if the incidence angle of light is

above the critical angle θ_c

$$\theta_c = \arcsin\left(\frac{n_2}{n_1}\right) \tag{1}$$

where n_1 and n_2 are the refractive indexes of core and cladding material, respectively. Moreover, the propagation of light obeys Snell's law

$$n_1 \sin(\theta_1) = n_2 \sin(\theta_2) \tag{2}$$

where θ_1 is the incidence angle and θ_2 is the refraction angle.

According to TIR, an optically clear silicone gel (Polymer Systems Technology Ltd., LS1-3252) is selected as the core material and its refractive index is 1.52. Ecoflex Gel (Smooth-On Inc.) is used to fabricate the cladding layer and its refractive index is 1.40. Thus, the critical angle is 67.08°. The greater the difference in the refractive index, the larger the critical angle, the less insertion loss. This parameter is useful to choose the light source with proper luminous angle. However, it lacks of intuitionistic when applied to the design of waveguide with complex trends. In this article, we focus on the influence of channel geometry parameters on macrobending. Light loss under different cross sections has been verified by simulation. The refraction coefficients of the core and cladding materials are consistent with those mentioned above. The schematic is shown in Fig. 1(a). All rays within the luminous angle (60°) of a point light source are set to have the same energy. The light source is fixed at the center of the input section of the waveguide. The overall light energy is 1 mW. The centerline of the waveguide is 30 mm with square cross section. The side length l is set as 0.5, 1, or 1.5 mm. The arc length of macrobending is 0.5 πR, where R is a natural number from 1 to 9 that represents the bending radius. The results are shown in Fig. 1(b), and the light intensity (a.u.) that is expressed as a percentage is a function of side length and bending radius of a waveguide. It is shown that the smaller the bending radius and the larger the side length of a waveguide, the smaller the light intensity (a.u.), since it is a scenario that gradually transitioned to microbending light loss.

With the proportionality coefficient (l/R) of side length and bending radius shown in Fig. 2 as the independent variable, macrobending light losses of optical waveguides with different cross sections are almost the same when the proportional coefficient remains constant. If the proportionality coefficient is less than 0.3, the macrobending light loss is less than 1%.

As for microbending that the radius is typically less than 1 mm [29], it is the deviation of the fiber profile from its ideal geometry. Microbending light loss is the working principle of the proposed sensor, which is used to establish the relationship between waveguide microdeformation and the pressure or, more precisely, a function between light loss and pressure. The key assumption of the proposed sensing method is that the embedded soft waveguide is almost volumetrically constant and has high elasticity. A pressure, applied on the tactile, causes a deformation of the waveguide and eventually light intensity loss due to the local reflection change. In addition, microbending is only allowed to occur by the contact force at the tactile.

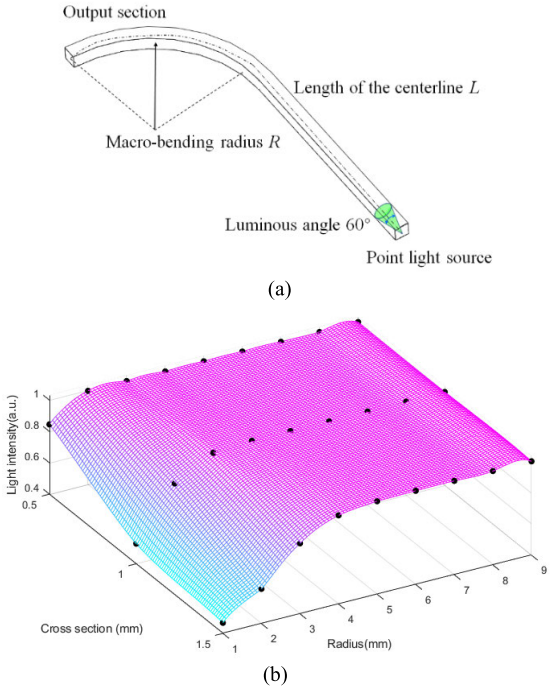

Fig. 1. Optical simulation to show the relationship between macrobending and light loss. (a) Schematic of a macrobending waveguide. (b) Light intensity (a.u.) is a function of side length and bending radius.

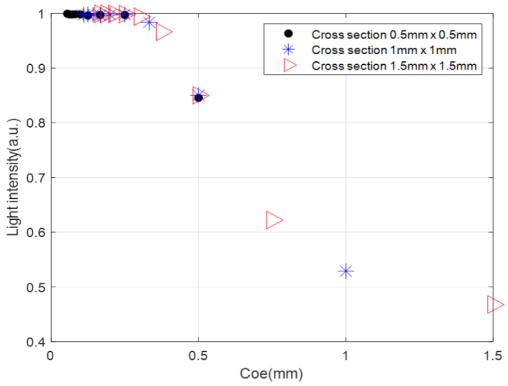

Fig. 2. Relationship between light intensity (a.u.) and proportionality coefficient, where the proportionality coefficient is the ratio of side length to bending radius of a waveguide.

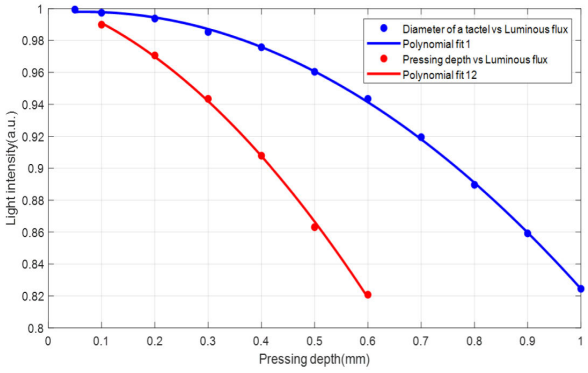

Fig. 3. Relationship between light intensity (a.u.) and the degree of microbending (blue solid line). Relationship between light intensity (a.u.) and pressing depth of the same tactile (red solid line).

In general, it is difficult to use a unified formula to express the microbending loss of a multimode fiber [30]. In this article,

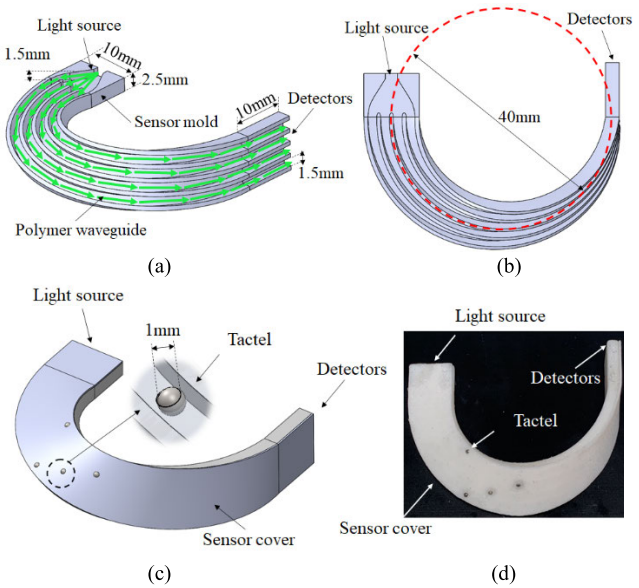

Fig. 4. Layout of the proposed distributed tactile sensor. (a) Optical path of the waveguide. (b) Diameter of macrobending. (c) Positions of tactiles on the 3-D complex surface. (d) Proposed sensor.

to verify the effect of microbending on light loss, two sets of simulations were carried out. The blue solid line represents the relationship between light intensity (a.u.) and the diameter of a tactile when the radius is taken as the pressing depth, as shown in Fig. 3, where the diameter is set to $0.05, 0.1, 0.2, \ldots,$ or 1 mm. It can be fit by a quadratic function (blue dashed line) $y = -0.1995x^2 + 0.0269x + 0.9970$ with R-square value 0.9996. Meanwhile, the red solid line represents the relationship between light intensity (a.u.) and pressing depth of the same tactile, as shown in Fig. 3. It is approximately linear. The red dashed line is the fitting curve $y = -0.3310x^2 - 0.1122x + 1.0050$, and the R-square value is 0.9991.

The above results that prove the feasibility of using spherical tactile combined with the resolution of the signal detector and the desired force range of the tactile sensor lay a basis for the selection of tactile size. In this article, the variation of light intensity (a.u.) should be as large as possible considering the errors in the fabrication process. Therefore, steel balls with a diameter of 1 mm are selected as tactiles and are fixed to the corresponding positions in the sensor cover using Ecoflex Gel. The cross section of the waveguide is square, as shown in Fig. 4.

Light loss always exists when light is injected into an optical waveguide, and using fewer injected points will help to improve energy efficiency. Therefore, the proposed sensor has the following structure: the light source is located at the root node, multiple signal detectors are located at the leaf nodes, and tactiles are distributed on the branches, as shown in Fig. 4. Linear camera is used as the detectors. Its specific type will be introduced in Section II-C. By adjusting the curvatures of different positions of each waveguide channel, the optical energy can be evenly distributed to each signal detector. The detailed simulation results will be given in Section II-A.2. The derivation process of this principle is shown as follows.

TABLE II
ENERGY EFFICIENCY OF THE PROPOSED SENSOR

	Power (mW)
Overall light energy	1
Output of channel 1	1.71E-1
Output of channel 2	1.71E-1
Output of channel 3	1.72E-1
Output of channel 4	1.84E-1
Energy efficiency	69.8%

Based on the law of energy conservation, ideally, the energy I_0 emitted from the light source is the sum of the energy of insertion loss I_{in}, the energy of macrobending loss of each branch $I_l(i)$, the energy of microbending loss of each tactile $I_p(i)$, and the received energy by each detector $I_d(i)$, which can be expressed as

$$I_0 = I_{\text{in}} + \sum_{i=1}^{m} \left(I_l\,(i) + I_p\,(i) + I_d(i)\right) \tag{3}$$

where m is the number of channels.

2) Sensor Design: In order to achieve arbitrary layout of tactiles with a good signal-to-noise ratio, various light losses of waveguide need to be considered.

On one hand, adverse light losses should be avoided during the manufacturing and assembling stages. Insertion loss can be minimized by injecting the light directly inside the input section of the channel. The effect of scattering losses, such as Rayleigh scattering, can be reduced by sufficiently stirring the solutions to reduce the possibility of uneven density of the core material so that the cured waveguide will exhibit structural homogeneity. Based on stereolithography 3-D printing technology, the micro-level resolution of the sensor base (0.025 mm) will guarantee a smooth surface of the core, which is useful to minimize surface scattering.

On the other hand, the light losses that have contributions to achieve tactile sensing and information transmission should be fully utilized, such as macrobending and microbending loss. Macrobending within the proportionality coefficient produces a negligible light loss. Therefore, on the premise of ensuring effective energy transfer efficiency, it is possible to design the waveguide circuit with single input and multiple outputs and extend this application to complex 3-D surfaces, in which branches with suitable curvatures are fundamental to decide the structure of the channels.

We assume that the radiant angle of the point light source is defined from 60° to 120°. Since the energy of a Lambertian illuminance distribution within this angle is very concentrated (around 75%, calculated by the optical simulation software Zemax), the input section gradually expands with an angle of 60°. After 10 mm, the waveguide begins to bifurcate into four channels. The cross section of each channel is slightly twisted along the direction of propagation but ends in a 1.5 × 1.5 mm. Overall, each channel has the macrobending of approximately 40 mm in diameter. The proportionality coefficient (l/R) of side length and bending radius is around 0.075.

Based on it, simulations of ray tracking were carried out, as shown in Fig. 5 and Table II. Notably, considering that the

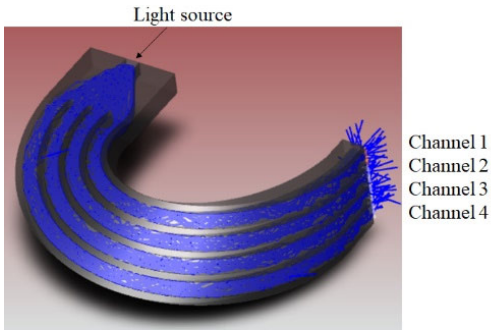

Fig. 5. Ray tracking by Zemax.

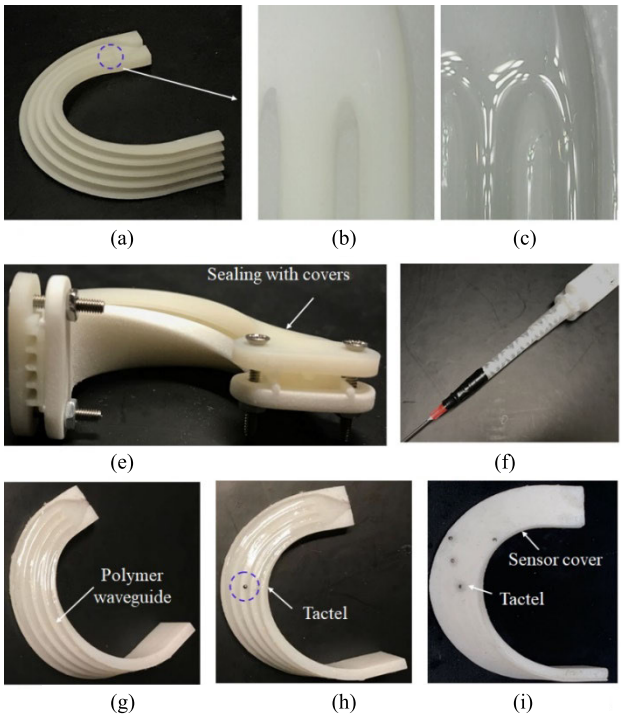

Fig. 6. Fabrication process of the polymer-based optical waveguide tactile sensing sensor for a 3-D surface. (a) Three-dimensional printed sensor mold. (b) Dip-coating in Ecoflex gel. (c) Sealing with channels. (d) Injecting LSI-3252. (e) Curing. (f) Assembling with the press buttons. (g) Encapsulating with a cover.

twisted angle between adjacent points is small compared to the length of the channel, this structure can maintain a good TIR. However, TIR is destroyed at the bifurcations, resulting in 69.8% energy utilization. The energy efficiency can be improved by changing the macrobending radius and adjusting the shape of the bifurcation. In addition, considering that the channels embedded in the proposed complex 3-D surface have similar length and curvature, a uniform light intensity distribution across all the channels can be obtained.

B. Fabrication Process and Procedure

To flexibly cope with various applications, we propose a fabrication process to embed the soft waveguide into channels of 3-D complex surface.

The steps are shown in Fig. 6, with instructions as follows.

1) The mold of waveguide is fabricated by 3-D printing technology.
2) The cladding layer is first manufactured by dip-coating the mold in Ecoflex Gel.
3) After curing at room temperature for 10–15 min, the exposed channels need to be sealed with covers tightly. In addition, if the input and output sections are not on the same level, the section with lower height should be sealed with wax because of its chemical stability and easy to remove, and a vent should be left to facilitate the discharge of internal bubbles.
4) Then, keeping the mold horizontally, LS1-3252 is injected into this container to form the core of the waveguide.
5) Still at room temperature, the polymer-based step-index multimode sensory waveguide will be obtained after 8–10 h.
6) Tactiles are placed on the expected positions of each channel. A rigid cover is assembled with the sensor mold to protect soft channels from dust and external light. Therefore, only the tactile area of waveguide is exposed to detect the pressure.
7) The cover layer and the sensor mold are glued together by Epoxy (Thorlabs Inc., G14250) because of its low corrosion to plastics.

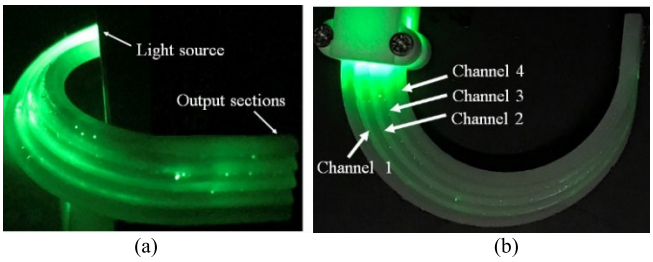

Fig. 7. (a) and (b) Optical images of the tactile sensors: light propagates along the channels of waveguide.

The optical image of the waveguide in the light-guide state is shown in Fig. 7. The light is capable to transmit along the designed channels. However, in the process of mixing and stirring the two constituent liquids of LS1-3252, a large number of trivial bubbles are generated in the solution, which are not discharged in full during injection. Therefore, the channel after solidification produced a large scattering of light, which affects the energy efficiency. This phenomenon can be observed through the glowing waveguide. It is a problem to be solved in the follow-up research.

C. Experimental Setup

The presented sensors are based on the measurement of light intensity modulation. As previously explained, normal forces applied on the sensor causes microbending in the structure of the waveguide, resulting in a light intensity decrease at the output section. The calibration experiments show the relationship between the loss of light intensity and pressure. Hysteresis, sensitivity, and dynamic testing experiments have been carried out to evaluate the sensor performances.

The aim of the experiments is to verify the feasibility of the proposed sensing principle and its fabrication method for embedding distributed haptic perception into a 3-D complex

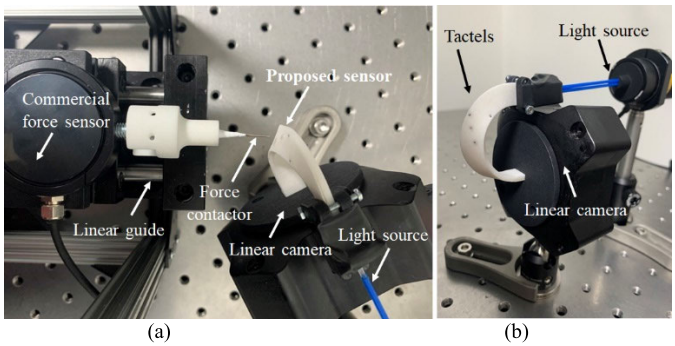

Fig. 8. (a) Calibration system: a force contactor that is connected with a commercial force sensor is driven by the linear guide. (b) Proposed sensing system. The input section of the proposed sensor is connected with an optical fiber, while the output section of the proposed sensor is connected with linear camera. The optical fiber that is connected with an LED is used as the light source.

surface. The experimental setup is shown in Fig. 8, which consists of a motorized linear guide (Newmark Systems Inc., ET-200-21), a load cell force sensor (Richmond Industries Ltd., 'S' Beam Load Cells of 900 Series), a linear camera (Thorlabs Ltd., LC100, 350–1100 nm, 2048 Pixel Linear Si charged-coupled device (CCD) Array), a light source (Thorlabs Ltd., M530L4–530 nm, 370 mW (Min) Mounted LED, 1000 mA), a force contactor, and the proposed sensors that are replaceable, in which the input section of the waveguide and light source is connected by a multimode optical fiber, while the output sections are directly contacted with CCD array of the linear camera. To avoid camera saturation of the light source, the integrating time of the linear camera is set as 20 ms. The prototype is calibrated with respect to the light loss of each channel. The force contactor points to the center of the tactile so that the actual normal force can be measured using the commercial sensor.

III. Experiments and Results

Evaluation experiments are carried out to demonstrate the feasibility of the above design as the tactile sensor. The linear guide with a force contactor (1 mm of diameter) moves along the normal direction of the tactile. During the calibration, the contact forces are recorded by the commercial force sensor, and meanwhile, the change in light intensity at the output section of the channels is collected by the linear camera. On the premise of not affecting the calibration results, the processing of light intensity is simplified. Considering that the cross section of each channel is a rectangle, only the observed signal of the CCD pixels of the linear camera corresponding to the centroid of the cross section is taken as the current value of light intensity.

The sensitivity of the proposed sensor is determined by the sensing pixel of linear camera. Therefore, this parameter can be obtained by calculating

$$S = \frac{\Delta X}{\Delta P} \tag{4}$$

where ΔX represents the change in light intensity by using the percentage value. Before normalization, at the maximum applied force, the light intensity from channels 1 to 4 varies in the range of 2.68%, 6.01%, 2.80%, and 1.00%,

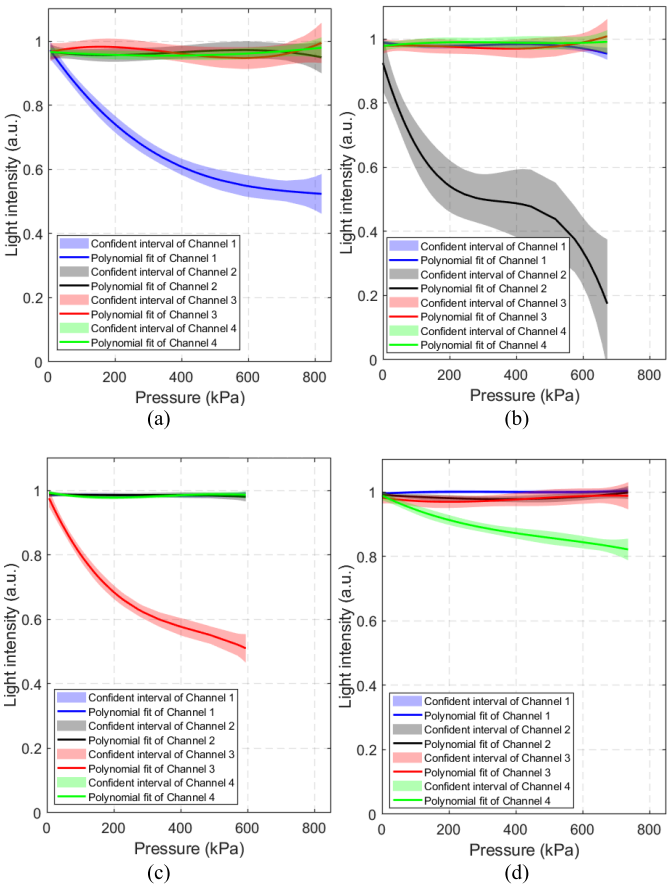

Fig. 9. Relationship between applied forces and light loss. The maximum measurement range is from 0 to 800 kPa. The loading and unloading process was repeated five times. The legend shows the meaning of each color. (a)–(d) Force contactor is acted on the tactile from channels 1 to 4, respectively.

respectively. ΔP represents its corresponding measurement range, which is 820, 673, 595, or 705 kPa. As a result, the sensitivities are 3.27×10^{-5} kPa^{-1}, 8.93×10^{-5} kPa^{-1}, 4.71×10^{-5} kPa^{-1}, and 1.42×10^{-5} kPa^{-1}.

After normalizing the light intensity with respect to the largest variation range (i.e., 6.01%), the calibration results of four tactiles for five repetitions are shown in Fig. 9, in which the blue, black, red, and green colors represent the data collected from channels 1 to 4, respectively. Semitransparent regions are 95% confidence intervals, and solid lines in the middle are fitting curves. To be more specific, for example, tactile from channel 1 is directly impacted by applied forces in Fig. 9(a), and changes in light intensity among all channels are detected by the linear camera simultaneously. Based on it, the crosstalk can be obtained, as shown in Table III. We found that other channels except channel 3 were less affected by crosstalk, with the maximum value not exceeding 6%. The reason for this phenomenon is that the light incident into the optical waveguide is not completely within the critical angle and may penetrate the cladding into other channels as it propagates. The position of tactile from channel 3 is closer to the output section of the optical waveguide. Therefore, the light escaping from the other tactiles is more likely to affect channel 3.

TABLE III
CROSSTALK AMONG ALL CHANNELS

Crosstalk \ Testing	tactel 1	tactel 2	tactel 3	tactel 4
Channel 1		4%	2%	6%
Channel 2	5%		2%	6%
Channel 3	9%	4%		12%
Channel 4	5%	1%	4%	

Because of the viscosity of the optical waveguide material, the loading and unloading curves cannot strictly coincide. The hysteresis of each tactile is calculated as follows:

$$H = \frac{\Delta Y}{Y} \times 100\% \tag{5}$$

where ΔY is the absolute value of the difference between the average value of output light intensity during unloading and loading and Y is the full range output. In this article, hysteresis uncertainties of all channels are 27%, 37%, 16%, and 39%.

The calibration curves are nonlinear. The possible explanation is given as follows. When the applied force is small, the sunk depth of the steel ball into the soft material channel is less than its radius. Due to the soil squeezing effect, the shallow soft material will be pushed to bulge, while the soft material in the deeper layer will be extruded laterally. The above changes show an increasing trend. Once the sunk depth exceeds the radius, the soft material located in the shallow layer will have the lateral movement to the position of the steel ball so that the deformation characteristics of the soft material will become complex so as to the transmission of light in the channel. The polynomial regression model is used to fit the experimental data. As long as the fitting curve is monotonic in the domain (i.e., the measurement range) to prevent the occurrence of multiple forces corresponding to one light intensity value, it is reasonable to choose any suitable fitting curve.

In addition, we also found that the initial values of light intensity across all the channels are different compared with simulation results because the random distribution of residual bubbles destroys TIR.

After that, the dynamic response of the proposed sensor was tested. The force contactor was driven to press tactiles with given frequencies and amplitudes. A combination of two frequencies (5 and 10 Hz) and two pressure ranges (from 450 to 850 kPa and from 450 to 650 kPa) are shown in this article. Data during 1 s are collected from linear camera and commercial force sensor. In Fig. 10, pressure on channel 1 is shown by the y-axis that is labeled on the left, while light intensity is shown by the y-axis that is labeled on the right. The results indicate that the proposed sensing method has good consistency and repeatability to track the dynamic signal. The average delay time of the phase response for given frequencies and amplitudes is around 12 ms.

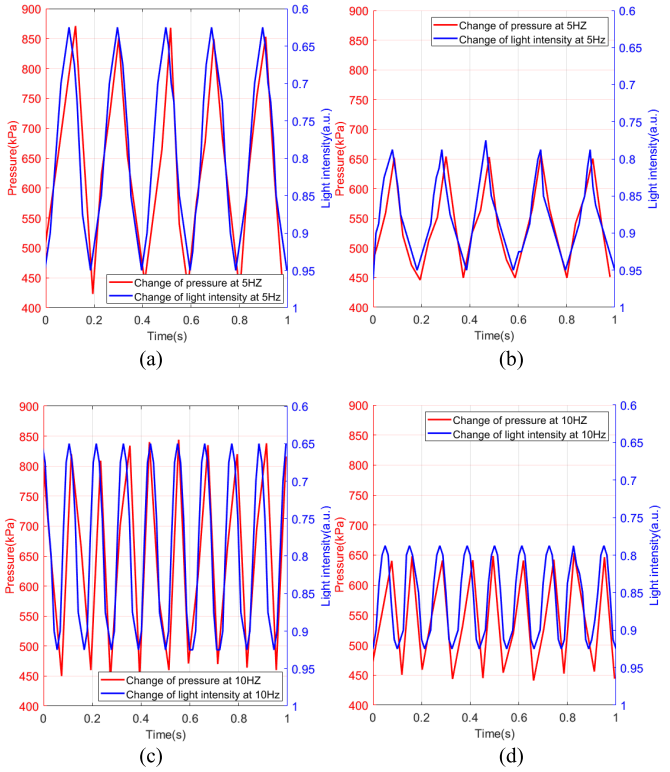

Fig. 10. Dynamic test for given frequencies. The delay time is around 12 ms. (a) Frequency: 5 Hz; pressure range: 450–850 kPa. (b) Frequency: 5 Hz; pressure range: 450–650 kPa. (c) Frequency: 10 Hz; pressure range: 450–850 kPa. (d) Frequency: 10 Hz; pressure range: 450–650 kPa.

IV. CONCLUSION AND DISCUSSION

In this article, we have proposed a novel polymer-based optical waveguide tactile sensing method to detect the normal pressure in a 3-D complex surface.

In order to obtain a good signal-to-noise ratio and achieve high tactile sensitivity, it is necessary to classify the factors causing waveguide losses to take advantage of necessary losses (such as microbending losses) and to suppress undesirable losses (such as macrobending losses and injection loss). Injection loss can be reduced by injecting light directly into the waveguide channel. When the bending radius of the waveguide becomes small enough that the propagation angle of the light is no longer applicable to TIR, a macrobending loss occurs. In the proposed design, the critical radius is around 8 mm. On the other side, we take advantage of microbending as a bridge to transform applied pressure to optical intensity output. Microbending determines the measurement range. Light loss caused by microbending determines the sensitivity. The recovery speed of microbending after removing the pressure determines the dynamic response ability.

The feasibility study of the polymer-based optical waveguide tactile sensor is validated in this article. The proposed tactile sensing method has the following advantages compared to other existing tactile sensing methods. First, an optical waveguide channel with a proper proportionality coefficient can be embedded in a complex 3-D surface. The waveguide is integrally formed along a channel. The positions of tactiles can be designed in a dispersed way across the curved surface. Second, the best sensing sensitivity for a tactile is 1.42×10^{-5} kPa^{-1}, the maximum measurement range is from 0 to 850 kPa, and the tactile can also rapidly response the signal change with a given frequency (10 Hz). The average delay time is around 12 ms.

REFERENCES

[1] Z.-Y. Chu, S.-B. Yan, J. Hu, and S. Lu, "Impedance identification using tactile sensing and its adaptation for an underactuated gripper manipulation," *Int. J. Control, Autom. Syst.*, vol. 16, no. 2, pp. 875–886, Apr. 2018.

[2] J. Konstantinova, A. Jiang, K. Althoefer, P. Dasgupta, and T. Nanayakkara, "Implementation of tactile sensing for palpation in robot-assisted minimally invasive surgery: A review," *IEEE Sensors J.*, vol. 14, no. 8, pp. 2490–2501, Aug. 2014.

[3] S. Luo, J. Bimbo, R. Dahiya, and H. Liu, "Robotic tactile perception of object properties: A review," *Mechatronics*, vol. 48, pp. 54–67, Dec. 2017.

[4] L. Zhu, Y. Xiang, Y. Liu, K. Geng, R. Yao, and B. Li, "Comparison of piezoelectric responses of flexible tactile sensors based on hydrothermally-grown ZnO nanorods on ZnO seed layers with different thicknesses," *Sens. Actuators A, Phys.*, vol. 341, Jul. 2022, Art. no. 113552.

[5] S. Wang, Y. Wang, Z. Chen, and D. Mei, "Kirigami design of flexible and conformal tactile sensor on sphere-shaped surface for contact force sensing," *Adv. Mater. Technol.*, vol. 8, no. 3, Feb. 2023, Art. no. 2200993.

[6] S. Akbarzadeh et al., "A simple fabrication, low noise, capacitive tactile sensor for use in inexpensive and smart healthcare systems," *IEEE Sensors J.*, vol. 22, no. 9, pp. 9069–9077, May 2022.

[7] P. Lu et al., "Distributed optical fiber sensing: Review and perspective," *Appl. Phys. Rev.*, vol. 6, no. 4, Sep. 2019, Art. no. 041302.

[8] N. F. Lepora, Y. Lin, B. Money-Coomes, and J. Lloyd, "DigiTac: A DIGIT-TacTip hybrid tactile sensor for comparing low-cost high-resolution robot touch," *IEEE Robot. Autom. Lett.*, vol. 7, no. 4, pp. 9382–9388, Oct. 2022.

[9] C. Yu, L. Lindenroth, J. Hu, J. Back, G. Abrahams, and H. Liu, "A vision-based soft somatosensory system for distributed pressure and temperature sensing," *IEEE Robot. Autom. Lett.*, vol. 5, no. 2, pp. 3323–3329, Apr. 2020.

[10] Z. Si and W. Yuan, "Taxim: An example-based simulation model for GelSight tactile sensors," *IEEE Robot. Autom. Lett.*, vol. 7, no. 2, pp. 2361–2368, Apr. 2022.

[11] H. Xie, H. Liu, Y. Noh, J. Li, S. Wang, and K. Althoefer, "A fiber-optics-based body contact sensor for a flexible manipulator," *IEEE Sensors J.*, vol. 15, no. 6, pp. 3543–3550, Jun. 2015.

[12] J. Hu, J. Back, P. Dasgupta, and H. Liu, "Embedding soft material channels for tactile sensing of complex surfaces—Mathematical modeling," *IEEE Sensors J.*, vol. 21, no. 3, pp. 3172–3183, Feb. 2021.

[13] S. J. Yoon, M. Choi, B. Jeong, and Y.-L. Park, "Elongatable gripper fingers with integrated stretchable tactile sensors for underactuated grasping and dexterous manipulation," *IEEE Trans. Robot.*, vol. 38, no. 4, pp. 2179–2193, Aug. 2022.

[14] M. N. Saadatzi, J. R. Baptist, Z. Yang, and D. O. Popa, "Modeling and fabrication of scalable tactile sensor arrays for flexible robot skins," *IEEE Sensors J.*, vol. 19, no. 17, pp. 7632–7643, Sep. 2019.

[15] A. Schmitz, M. Maggiali, L. Natale, B. Bonino, and G. Metta, "A tactile sensor for the fingertips of the humanoid robot iCub," in *Proc. IEEE/RSJ Int. Conf. Intell. Robots Syst.*, Taiwan, Oct. 2010, pp. 2212–2217.

[16] W. Xiao, F. Sun, H. Liu, H. Liu, and C. He, "Dexterous robotic hand grasp modeling using piecewise linear dynamic model," in *Proc. IEEE Int. Conf. Multisensor Fusion Integr. Intell. Syst. (MFI)*, Hamburg, Germany, Sep. 2012, pp. 52–57.

[17] C. Wang, C. Wang, Z. Huang, and S. Xu, "Materials and structures toward soft electronics," *Adv. Mater.*, vol. 30, no. 50, Dec. 2018, Art. no. 1801368.

[18] B. Wang and A. Facchetti, "Mechanically flexible conductors for stretchable and wearable e-skin and e-textile devices," *Adv. Mater.*, vol. 31, no. 28, Jul. 2019, Art. no. 1901408.

[19] N. Yogeswaran et al., "New materials and advances in making electronic skin for interactive robots," *Adv. Robot.*, vol. 29, no. 21, pp. 1359–1373, 2015.

[20] P. Won et al., "Stretchable and transparent kirigami conductor of nanowire percolation network for electronic skin applications," *Nano Lett.*, vol. 19, no. 9, pp. 6087–6096, Sep. 2019.

[21] A. Pagoli, F. Chapelle, J.-A. Corrales-Ramon, Y. Mezouar, and Y. Lapusta, "Large-area and low-cost force/tactile capacitive sensor for soft robotic applications," *Sensors*, vol. 22, no. 11, p. 4083, May 2022.

[22] S. Kang et al., "Transparent and conductive nanomembranes with orthogonal silver nanowire arrays for skin-attachable loudspeakers and microphones," *Sci. Adv.*, vol. 4, no. 8, Aug. 2018, Art. no. eaas8772.

[23] T. Bu et al., "Stretchable triboelectric-photonic smart skin for tactile and gesture sensing," *Adv. Mater.*, vol. 30, no. 16, Apr. 2018, Art. no. 1800066.

[24] J. Yu et al., "Highly skin-conformal wearable tactile sensor based on piezoelectric-enhanced triboelectric nanogenerator," *Nano Energy*, vol. 64, Oct. 2019, Art. no. 103923.

[25] S.-Z. Guo, K. Qiu, F. Meng, S. H. Park, and M. C. McAlpine, "3D printed stretchable tactile sensors," *Adv. Mater.*, vol. 29, no. 27, 2017, Art. no. 1701218.

[26] D.-H. Kim et al., "Dissolvable films of silk fibroin for ultrathin conformal bio-integrated electronics," *Nature Mater.*, vol. 9, no. 6, pp. 511–517, Jun. 2010.

[27] P. Wang et al., "Biocompatible and self-healing ionic gel skin as shape-adaptable and skin-adhering sensor of human motions," *Chem. Eng. J.*, vol. 398, Oct. 2020, Art. no. 125540.

[28] S. Wang et al., "Skin electronics from scalable fabrication of an intrinsically stretchable transistor array," *Nature*, vol. 555, no. 7694, pp. 83–88, 2018.

[29] J. Jay, "An overview of macrobending and microbending of optical fibers," Corning Incorporated, One Riverfront Plaza, Corning, NY, USA, 2010. [Online]. Available: https://www.corning.com/media/worldwide/coc/documents/Fiber/white-paper/WP1212.pdf

[30] Y. Liao, *Fiber Optics*. Beijing, China: Tsinghua Univ. Press, 2000, pp. 95–96.

Jian Hu is an Assistant Professor with the Chinese Academy of Sciences, Institute of Automation (CASIA), and the Centre of AI and Robotics (CAIR), Hong Kong Institute of Science and Innovation, Chinese Academy of Sciences, Beijing, China. His research focuses on the development of medical robotic systems with advanced haptic perception.

Danqian Cao is pursuing the Ph.D. degree with the School of Biomedical Engineering and Imaging Sciences, Faculty of Life Sciences and Medicine, King's College London, London, U.K. Her doctoral research is focused on soft robotics' haptic perception based on photoacoustic and low coherence interferometry.

Yue Li is pursuing the Ph.D. degree with the School of Biomedical Engineering and Imaging Sciences, Faculty of Life Sciences and Medicine, King's College London, London, U.K.

Her research interests include haptic perception and its circuit design.

Hongbin Liu is a Professor with the Chinese Academy of Sciences, Institute of Automation (CASIA), and the Executive Deputy Director of the Centre of AI and Robotics (CAIR), Hong Kong Institute of Science and Innovation, Chinese Academy of Sciences, Beijing, China. He is also an Adjunct Reader and the Director of the Haptic Mechatronics and Medical Robotics (HaMMeR) Laboratory, School of Biomedical Engineering and Imaging Sciences, King's College London (KCL), London, U.K. His group has been focusing on research and development of medical robotic systems with advanced haptic perception and interaction capabilities, to enable safer and more effective minimally invasive diagnosis and treatment for patients. His research has led to the clinical translation of a series of flexible robotic endoscopic systems for applications such as colonoscopy, bronchoscopy, and vascular surgeries.